


Cite this: *RSC Adv.*, 2023, 13, 28729

# Porous acid–base hybrid polymers for enhanced NH<sub>3</sub> uptake with assistance from cooperative hydrogen bonds†

Xiaoyan Luo,<sup>a</sup> Yibang Liu,<sup>a</sup> Mingxing Li,<sup>a</sup> Renhui Ling,<sup>a</sup> Ling Ye,<sup>a</sup> Xuegong Cao<sup>a</sup> and Congmin Wang<sup>a,b</sup>

Carboxylic acid-modified materials are a common means of achieving efficient NH<sub>3</sub> adsorption. In this study, we report that improved NH<sub>3</sub> adsorption capacity and easier desorption can be achieved through the introduction of substances containing Lewis basic groups into carboxylic acid-modified materials. Easily synthesized mesoporous acid–base hybrid polymers were constructed with polymers rich in carboxylic acid and Lewis base moieties through cooperative hydrogen bonding interactions (CHBs). The hybrid polymer PAA–P4VP presented higher NH<sub>3</sub> capacity (18.2 mmol g<sup>−1</sup> at 298 K and 1 bar NH<sub>3</sub> pressure) than PAA (6.0 mmol g<sup>−1</sup>) through the acid–base reaction and the assistance from CHBs with NH<sub>3</sub>, while the NH<sub>3</sub> desorption from PAA–P4VP was easier for the reformation of CHBs. Based on the introduction of CHBs, a series of mesoporous acid–base hybrid polymers was synthesized with NH<sub>3</sub> adsorption capacity of 15.8–19.3 mmol g<sup>−1</sup> and high selectivity of NH<sub>3</sub> over CO<sub>2</sub> ( $S_{\text{NH}_3/\text{CO}_2} = 25.4\text{--}56.3$ ) and N<sub>2</sub> ( $S_{\text{NH}_3/\text{N}_2} = 254\text{--}1068$ ), and the possible co-existing gases, such as SO<sub>2</sub>, had a lower effect on NH<sub>3</sub> uptake by hybrid polymers. Overall, the hybrid polymers present efficient NH<sub>3</sub> adsorption owing to the abundant acidic moieties and CHBs, while the concomitant Lewis bases promote NH<sub>3</sub> desorption.

Received 7th August 2023  
Accepted 15th September 2023

DOI: 10.1039/d3ra05346f

rsc.li/rsc-advances

## Introduction

Ammonia (NH<sub>3</sub>) is indispensable in our lives today for producing artificial fertilizers and several military and commercial products, including explosives, refrigerants, pharmaceuticals, and synthetic fibers. NH<sub>3</sub> is also a potential fuel, providing a way to store and transport hydrogen owing to its exploitable energy density. However, the unavoidable leakage of NH<sub>3</sub> during its utilization has huge adverse impacts on the environment and human health. In these applications associated with the critical risks of this gas, effective adsorbents possessing the ability to store more NH<sub>3</sub> have been attracting substantial attention.

Porous materials with high surface areas, such as active carbon<sup>1</sup> and zeolites,<sup>2–4</sup> have been used as NH<sub>3</sub> adsorbents; however, they suffer from relatively low affinity and limited capacity for NH<sub>3</sub>. Simultaneously, porous materials, including metal–organic frameworks (MOFs),<sup>5,6</sup> porous organic polymers

(POPs),<sup>7</sup> covalent organic frameworks (COFs),<sup>8</sup> and hydrogen-bonded organic frameworks (HOFs),<sup>9</sup> were developed as efficient NH<sub>3</sub> adsorbents owing to their highly porous nature, strong stability, and designable abundant binding sites.<sup>10</sup> The modification of porous materials with functionalized moieties was expected to result in superior adsorbed amounts. Functionalized UiO-66-A/B/C<sup>11</sup> and UiO-66-ox synthesized *via* post-synthetic modification with free carboxylic acids indicated their positive utilization in NH<sub>3</sub> capture,<sup>12</sup> likewise the NH<sub>3</sub> adsorption performance of Zr-based UiO-66 analogues.<sup>13,14</sup> Various Brønsted acidic groups, such as –CO<sub>2</sub>H and –SO<sub>3</sub>H, were used to functionalize the water-stable framework UiO-66 and were reported with improved NH<sub>3</sub> capacity.<sup>15</sup> Acid-loaded porphyrin-based MOFs<sup>16</sup> for capturing NH<sub>3</sub> show remarkable stability and the isorecticular porphyrin-based MOFs<sup>17</sup> were reported with rod-like secondary building units of Brønsted acid bridging hydroxyl groups for NH<sub>3</sub> sorption. Similarly, the zirconium-based MOF, NU-300 with free Brønsted acid sites benefited the binding of NH<sub>3</sub> even at low pressures.<sup>18</sup> Recently, carboxylic-functionalized mesoporous copolymers PDVB-xAA were developed for fast, highly efficient, selective, and reversible NH<sub>3</sub> adsorption.<sup>19</sup> These studies revealed that NH<sub>3</sub> capture relies on the interplay of the functional groups, especially the –COOH of adsorbents.

It was found that the COFs modified with weak acid groups and hydrogen bonding interactions presented more efficient NH<sub>3</sub> uptake than strong acid-functionalized COFs. BBP-5, a COF

<sup>a</sup>Xiamen Key Laboratory of Optoelectronic Materials and Advanced Manufacturing, Key Laboratory of Molecular Designing and Green Conversions (Fujian Province University), College of Materials Science and Engineering, Huaqiao University, Xiamen 361021, P.R. China. E-mail: chemistryxy@163.com

<sup>b</sup>Department of Chemistry, Center of Chemistry for Frontier Technologies, Zhejiang University, Hangzhou 310027, P. R. China. E-mail: chewcm@zju.edu.cn

† Electronic supplementary information (ESI) available. See DOI: <https://doi.org/10.1039/d3ra05346f>



with carboxylate acid group showed more efficient and reversible  $\text{NH}_3$  uptake than PPN-6- $\text{SO}_3\text{H}$  due to the existence of cooperative hydrogen bonds (CHBs) along with the acid-Lewis base interactions between carboxylic acid and  $\text{NH}_3$ , which indicated that multiple chemical interactions were optimized to single strong interactions.<sup>20</sup> Similarly, urea-functionalized Zn-MOFs with an increased number of hydrogen bonds<sup>21</sup> were also reported to have outstanding  $\text{NH}_3$  adsorption. HOFs, mainly constructed by the self-assembly of organic molecules *via* intermolecular hydrogen bonding interactions, were explored as a potential corrosive gas trapping agent because of their abundant CHBs and porous structure. Jancik<sup>22</sup> explored UNAM-1 constructed of hydrogen-bonded frameworks, which achieved the porosity required for reversible  $\text{SO}_2$  uptake. Kang<sup>9</sup> reported a hydrogen-bonded network KUF-1 for  $\text{NH}_3$  capture with a sigmoidal adsorption isotherm and achieved the  $\text{NH}_3$  capacity of  $6.67 \text{ mmol g}^{-1}$  at 1 bar. They found that the design of an adsorbent/absorbent with a flexible hydrogen bonding network presented superior  $\text{NH}_3$  capacity and desorption regeneration. However, the refined design and cost-intensive synthesis of MOFs, COFs, and HOFs are very real problems against their application.

It was found that the hydrogen bonding interactions between the ionic liquids (ILs) and  $\text{NH}_3$  were the key to the significant increase in  $\text{NH}_3$  capacity according to Palomar's work.<sup>23</sup> Therefore, protic ILs<sup>24,25</sup> and ILs substituted with hydroxyl groups,<sup>23,26</sup> and poly ionic liquids (PILs) served as adsorbents of ammonia.<sup>27,28</sup> In our previous work,<sup>29,30</sup> amidine and pyridine-based protic ILs constructed with CHBs presented sigmoidal isotherms, and the results indicated a high  $\text{NH}_3$  capacity of  $7.5\text{--}9.3 \text{ mmol g}^{-1}$  at 1 bar,  $30^\circ\text{C}$ ; furthermore, the threshold pressure could be regulated through the CHBs. Deep eutectic solvents (DESs), known as new ILs analogues, consist of hydrogen bond acceptors (HBA) and hydrogen bond donors (HBD) in suitable molar ratios based on hydrogen bonding interactions and other intermolecular noncovalent interactions.<sup>31–38</sup> It has been proposed that DESs are very promising  $\text{NH}_3$  absorbents through Lewis acid–base and hydrogen bonding interactions.<sup>39</sup> For instance, choline chloride-composed DESs were developed for  $\text{NH}_3$  absorbents,<sup>40–42</sup> and choline chloride/resorcinol/glycerol (1 : 3 : 5) presented the  $\text{NH}_3$  absorption capacity of 13 wt% at 313.2 K and 0.1 MPa for the internal hydrogen-bonded network of DESs.<sup>40</sup> Alcohol, phenol,<sup>43,44</sup> and sugar<sup>45</sup> were also selected as components of DESs by taking advantage of their hydroxyl groups for effective  $\text{NH}_3$  absorption. Protic DESs with  $\text{NH}_4\text{SCN}$ , ethylamine hydrochloride and ethanolamine hydrochloride as HBAs were reported as excellent  $\text{NH}_3$  absorbents through strong hydrogen bonding interactions,<sup>46,47</sup> and the influences of HBA of DESs on the  $\text{NH}_3$  absorption performances were systematically investigated. According to the weak acidity of azole, azole-based DESs were also used as  $\text{NH}_3$  absorbents;<sup>48–50</sup> it was found that the greater acidity of the azole benefited the  $\text{NH}_3$  capacity but went against the reversibility.<sup>51</sup> Recently, it was reported that DESs involving metal chlorides including  $\text{LiCl}$ ,<sup>52</sup>  $\text{M(II)Cl}_2$ ,<sup>53,54</sup> and  $\text{M(III)Cl}_3$ ,<sup>53</sup> could achieve greater  $\text{NH}_3$  capacity for the coordination of  $\text{NH}_3$  with metal and hydrogen bonding

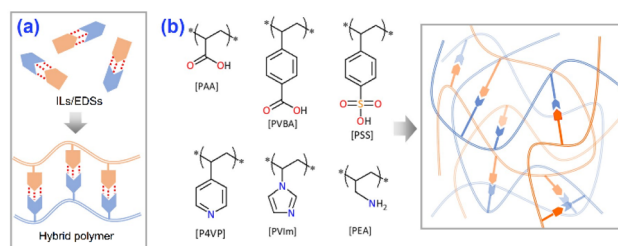


Fig. 1 (a) A diagram showing the idea of developing acid–base hybrid polymers for  $\text{NH}_3$  uptake. (b) Structures of the agents used for synthesizing hybrid polymers.

interactions. For instance, it was found that the CHBs-rich ILs/DESs had a good trapping effect on  $\text{NH}_3$ , while the  $\text{NH}_3$  absorption capacity would be enhanced by 18.1–36.9% when a small amount of metal chlorides was added to Res/EG (1 : 2) DES.<sup>54</sup>

The reports of sorbents substituted with carboxylic acid for efficient  $\text{NH}_3$  adsorption and the utilization of hydrogen bonds to improve  $\text{NH}_3$  desorption inspired us to construct self-assembled hybrid polymers based on the formation of CHBs between carboxylate acids and Lewis bases (Fig. 1a), which would enhance the affinity for  $\text{NH}_3$  as well as promote  $\text{NH}_3$  desorption by the reconstruction of CHBs. To obtain this target, various acid–base hybrid polymers (Fig. 1b) were explored to analyze the effects of the interactions between acidic and basic groups on  $\text{NH}_3$  uptake.

## Results and discussion

The reagents, preparation and characterization of hybrid polymers, and the  $\text{NH}_3$  adsorption and desorption experiments are described in the ESI File† in detail.

### The characterization of hybrid polymers

To explore the feasibility of the utilization of CHBs in enhancing the  $\text{NH}_3$  uptake by acid–base hybrid polymers, PAA and PVBA with carboxylic acid groups were hybridized with P4VP/PVIm containing Lewis base groups to synthesize hybrid polymers as  $\text{NH}_3$  adsorbents. The CHBs were further proposed from the optimized structures calculated through the DFT method as shown in Fig. S2.† The interaction energies between these acid and basic moieties were between  $-40.23$  and  $-46.90 \text{ kJ mol}^{-1}$  as listed in Table 1, which allows the possibility to self-assemble the acid–base hybrid polymers. For PAA–P4VP, the interactions between PAA and P4VP were calculated through propionic acid and 4-ethylpyridine, the reaction enthalpy was  $-40.23 \text{ kJ mol}^{-1}$  and the Gibbs free energy was  $-1.28 \text{ kJ mol}^{-1}$ , which indicate the possibility of interaction between PAA and P4VP.

The elemental contents of C, N, and H listed in Table S1† correspond with the theoretical data calculated from the molar ratio of acid and base moieties of 1 : 1, indicating that the hybrid polymers self-assemble in the equimolar reaction of  $-\text{COOH}$  and Lewis base. The IR spectra of acid–base hybrid polymers in Fig. S3† exhibit the changes in the vibration of



**Table 1** The interaction energies between acidic and basic groups and the  $\text{NH}_3$  desorbed active energy from the TPD test

| Entry | Complex   | Interaction energy <sup>a</sup> (kJ mol <sup>-1</sup> ) | TDP peak (°C) | Desorbed active energy <sup>b</sup> (kJ mol <sup>-1</sup> ) |
|-------|-----------|---|---------------|---|
| 1     | PAA-P4VP  | -40.23  | 78            | 104.0   |
| 2     | PAA-PVIm  | -46.90  | 90            | 107.6   |
| 3     | PVBA-P4VP | -40.05  | 75            | 103.2   |
| 4     | PVBA-PVIm | -46.75  | 87            | 106.8   |
| 5     | PAA       | —   | 112           | 114.3   |

<sup>a</sup> The interaction energies between acidic and basic groups were obtained through DTF calculations on the B3LYP basis set at the 6-31G++ level.<sup>b</sup> The active energies of  $\text{NH}_3$  desorption were calculated based on the Redhead method<sup>55</sup> according to the desorption temperature from  $\text{NH}_3$ -TPD.

$\text{C}=\text{O}$  as compared with acid polymers for the formation of CHBs. The IR spectra of PAA and PAA-P4VP in Fig. S3a† show that the stretching vibration of  $-\text{COOH}$  at  $1698\text{ cm}^{-1}$  was blue shifted to  $1713\text{ cm}^{-1}$  with the hybridization with P4VP (marked with a star). According to the 2D correlation IR spectra in Fig. S4,† the absorption of  $\nu(\text{COOH})$  was correlated with the vibration of the pyridine group at about  $1600\text{ cm}^{-1}$  (marked with a red star), which indicates the interaction between PAA and P4VP.

The SEM images in Fig. 2a present the mesoporosity of these hybrid polymers. The BET surface areas of hybrid polymers according to  $\text{N}_2$  adsorption at 77 K in Fig. 2b and S5† range from  $11.2$  to  $23.6\text{ m}^2\text{ g}^{-1}$  (Table 2) and their pore size distribution is  $2\text{--}30\text{ nm}$ , which explains the mesoporous structure of these hybrid polymers. On comparison of the SEM images and  $\text{N}_2$  adsorptions of nonporous PAA in Fig. S6b† and 2b, it was concluded that the porosity of PAA-P4VP was due to the multiple interactions between PAA and P4VP.

### $\text{NH}_3$ uptake of PAA-P4VP vs. pure PAA

It was reported that materials rich in CHBs are suitable for efficient  $\text{NH}_3$  uptake; thus, hybrid polymers were used for  $\text{NH}_3$  uptake. Interestingly, PAA-P4VP presents a higher  $\text{NH}_3$  uptake capacity of  $18.2\text{ mmol g}^{-1}$  than PAA ( $6.0\text{ mmol g}^{-1}$ ) from Fig. 3a, and the  $\text{NH}_3$  trapped in PAA-P4VP would be released feasibly. From the reported data according to the properties of DESSs, ILs, and acid-modified MOFs listed in Table S2,† the hybrid polymer showed excellent  $\text{NH}_3$  uptake capacity and mild desorption conditions. The comparison of the IR spectra of fresh and  $\text{NH}_3$  saturated samples in Fig. 3b indicates that  $-\text{COOH}$  reacts with  $\text{NH}_3$  to form  $-\text{COONH}_4$  according to the vibration of  $-\text{COO}^-$  at

$1500\text{ cm}^{-1}$ , and new peaks at  $850\text{ cm}^{-1}$  (marked with #) ascribed to the hydrogen-bonded  $\text{NH}_3$ .<sup>19</sup> From the  $\text{NH}_3$ -TPD detection curve in Fig. 3c, the most ammonia was released from PAA-P4VP when the temperature reached  $78\text{ }^\circ\text{C}$ , while the  $\text{NH}_3$  desorption peak occurred at  $112\text{ }^\circ\text{C}$  for PAA, indicating that the  $\text{NH}_3$  release from PAA-P4VP was easier. It should be noted the peaks at about  $200\text{ }^\circ\text{C}$ , which arise from polymer fragments, collapsed according to the TGA results as shown in Fig. S6;† this indicates that the weights of PAA and PAA-P4VP begin to decline from  $207$  and  $198\text{ }^\circ\text{C}$ , respectively. The comparison of the IR spectra of the fresh and recovered samples after  $\text{NH}_3$  desorption in Fig. 3b indicates that the PAA-P4VP could be recovered, and it is probably facilitated by the exothermic CHB formation between PAA and P4VP.<sup>29,56</sup> The  $-\text{COONH}_4$  remains in PAA for the obvious absorption of  $\text{COO}^-$  at  $1540\text{ cm}^{-1}$  (marked with pink shadow), which demonstrates the better properties of PAA-P4VP as an  $\text{NH}_3$  adsorbent as compared to PAA. For 8 consecutive cycles of  $\text{NH}_3$  adsorption-desorption experiments (Fig. 3d), the efficient  $\text{NH}_3$  capacity of PAA-P4VP remained steady while there was an obvious decrease for PAA, which might be due to part of the unrecovered carboxylic acid in PAA. The uptake of  $\text{NH}_3$  and other gases by PAA-P4VP in Fig. S7† shows that there was not considerable  $\text{CO}_2$  or  $\text{N}_2$  adsorption, and the selectivity of  $\text{NH}_3$  as compared to  $\text{CO}_2$  and  $\text{N}_2$  was  $54.0$  and  $408$ , respectively. As can be seen, the acid-base hybrid polymer PAA-P4VP presented enhanced  $\text{NH}_3$  adsorption and desorption as compared with PAA and high selectivity for  $\text{NH}_3$ , which indicate the potential application of acid-base polymers as  $\text{NH}_3$  adsorbents.

### The effects of CHBs on the $\text{NH}_3$ uptake of PAA-P4VP

To investigate the effects of P4VP on the  $\text{NH}_3$  uptake of PAA-P4VP, other complexes including PAA-BPY and PAA-PS were synthesized (Fig. S8a†). PS has the same chainlike structure like P4VP but without the Lewis base moieties, while BPY has the same Lewis base moieties as P4VP. The PAA-BPY and PAA-PS are non-porous as seen from the SEM in Fig. S8b,† which indicates that the Lewis base moieties and the chainlike structure are important for forming porous complexes. The FT-IR spectra in Fig. S9a† show a blue shift of  $\nu(\text{COOH})$  when PAA reacts with BPY but it was less affected by PS, indicating the formation of the CHBs between PAA and BPY. The  $\text{NH}_3$  uptake properties from Fig. S10† show that the adsorption capacity and desorption of PAA-PS are close to those of PAA, indicating that there

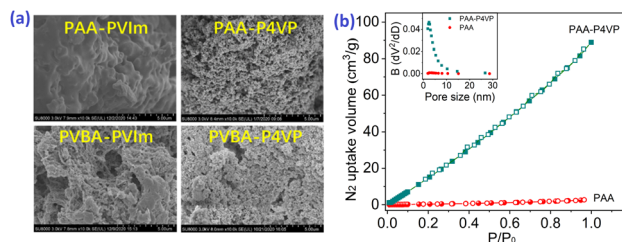


**Fig. 2** (a) The SEM images of hybrid polymers. (b) The  $\text{N}_2$  adsorption isotherm curve at 77 K and the pore distribution (inner picture) of PAA and PAA-P4VP.



Table 2 The BET surface areas and gas uptake capacities of hybrid polymers and PAA

| Entry | Complex   | $S_{\text{BET}}^a$ ( $\text{m}^2 \text{g}^{-1}$ ) | Gas capacity ( $\text{mmol g}^{-1}$ ) |                |                 | Selectivity <sup>d</sup> |                           |
|-------|-----------|---|---------------------------------------|----------------|-----------------|--------------------------|---------------------------|
|       |           |   | $\text{NH}_3^b$                       | $\text{N}_2^c$ | $\text{CO}_2^c$ | $\text{NH}_3/\text{N}_2$ | $\text{NH}_3/\text{CO}_2$ |
| 1     | PAA-P4VP  | 23.6  | 18.2                                  | 0.0445         | 0.396           | 408                      | 54.0                      |
| 2     | PAA-PVIm  | 11.2  | 19.3                                  | 0.0181         | 0.398           | 1068                     | 48.6                      |
| 3     | PVBA-P4VP | 23.0  | 18.4                                  | 0.0723         | 0.557           | 254                      | 33.0                      |
| 4     | PVBA-PVIm | 23.6  | 15.8                                  | 0.0478         | 0.622           | 331                      | 25.4                      |
| 5     | PAA       | 0.7   | 6.0                                   | —              | —               | —                        | —                         |

<sup>a</sup> The specific surface areas were calculated by the Brunauer–Emmett–Teller equation according to the  $\text{N}_2$  adsorption–desorption isotherm at 77 K.

<sup>b</sup> The  $\text{NH}_3$  uptake was operated under the self-made device at 25 °C. <sup>c</sup> The  $\text{N}_2$  and  $\text{CO}_2$  adsorptions were detected via Micromeritics BAFLEX surface characterization measurements at 25 °C. <sup>d</sup> The selectivity of  $\text{NH}_3$  over  $\text{N}_2$  ( $\text{CO}_2$ ) was calculated based on the capacity of  $\text{NH}_3$  divided by the capacity of  $\text{N}_2$  ( $\text{CO}_2$ ).

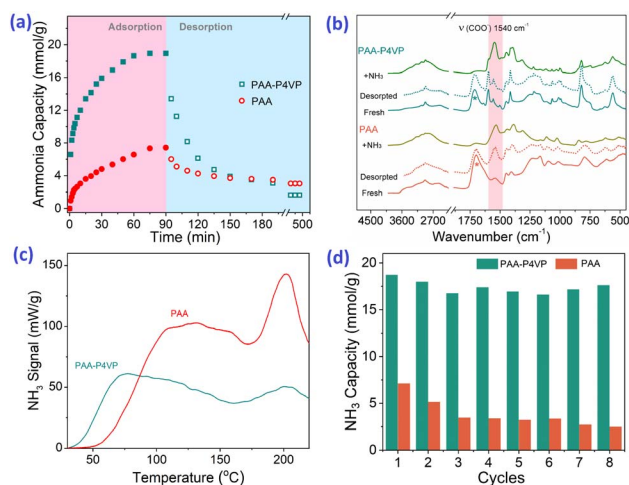


Fig. 3 (a) The  $\text{NH}_3$  uptake and residual capacity of PAA and PAA–P4VP with time. (b) FT-IR spectra of fresh,  $\text{NH}_3$  saturated, and recovered PAA and PAA–P4VP. (c)  $\text{NH}_3$ -TPD curves of PAA and PAA–P4VP with temperature increase ratio of 2 °C  $\text{min}^{-1}$  to 220 °C. (d) 8 consecutive  $\text{NH}_3$  adsorption–desorption results for PAA and PAA–P4VP.  $\text{NH}_3$  uptake at 25 °C, 1 bar.  $\text{NH}_3$  desorption at 80 °C under vacuum.

was no obvious improvement in the  $\text{NH}_3$  uptake of PAA for the mixture of PS. The  $\text{NH}_3$  capacity of PAA-BPY was 13.0  $\text{mmol g}^{-1}$  and just 1.5  $\text{mmol NH}_3 \text{g}^{-1}$  remained after desorption under vacuum at 80 °C for 90 min. The superior properties of PAA-BPY as compared to PAA-PS indicate that the insertion of Lewis base moieties benefits  $\text{NH}_3$  uptake capacity and desorption, and the competitive formation of CHBs between carboxylic acid and pyridine groups, which implies that the hybrid polymers are excellent ammonia sorbents.

### $\text{NH}_3$ uptake of acid–base hybrid polymers

Based on the strategy of developing acid–base hybrid polymers for improved  $\text{NH}_3$  uptake, hybrid acid–base polymers constructed with PAA and PVBA as acid polymers, P4VP and PVIm as Lewis base polymers were synthesized to investigate the effects of the interactions between acid and base moieties on  $\text{NH}_3$  uptake properties. These hybrid polymers were used for  $\text{NH}_3$  uptake at 1 bar and 25 °C; their  $\text{NH}_3$  capacity was 15.8–

19.3  $\text{mmol g}^{-1}$  from Fig. 4a and most of the fixed  $\text{NH}_3$  could be desorbed under vacuum at 80 °C for 100 min. Simultaneously, the  $\text{N}_2$  and  $\text{CO}_2$  adsorption by the hybrid polymers was also measured at 1 bar and 25 °C, which showed that tiny amounts of  $\text{CO}_2$  but non-considerable  $\text{N}_2$  could be adsorbed, as shown in Table 2. The selectivity of  $\text{NH}_3$  as compared to  $\text{CO}_2$  and  $\text{N}_2$  was 25.4–54.0 and 254–1068, respectively, which suggests the potential for the efficient separation of  $\text{NH}_3$  from these mixture gases. Besides, some interfering gases are inevitably present in industry, and the effects of the adsorbed  $\text{CO}_2$ ,  $\text{SO}_2$ , and  $\text{H}_2\text{O}$  on  $\text{NH}_3$  uptake were investigated. Fig. 4b shows that 18.44  $\text{mmol g}^{-1}$   $\text{NH}_3$  would be fixed after 0.77  $\text{mmol g}^{-1}$   $\text{SO}_2$  adsorption of PAA–P4VP, and the same phenomenon for  $\text{CO}_2$ , which indicates no obvious effect of the acid gas on the  $\text{NH}_3$  uptake by PAA–P4VP. There was a considerable  $\text{H}_2\text{O}$  uptake capacity of 7.22  $\text{mmol g}^{-1}$  by PAA–P4VP but the subsequent ammonia adsorption capacity was reduced to 16.71  $\text{mmol g}^{-1}$ , likely due to the active hydrogen bonding sites being occupied by  $\text{H}_2\text{O}$ .

The capacity of acid–basic hybrid polymers is susceptible to ammonia pressure and temperature; from Fig. 5, the  $\text{NH}_3$  capacity decreases along with the increase in temperature and decrease in  $\text{NH}_3$  pressure, which indicates that the  $\text{NH}_3$  would be desorbed with the variation of temperature and pressure. It should be noted that there were uptake plateaus at  $P/P_0 = 0.05$  of PAA–P4VP and  $P/P_0 = 0.2$  of PAA–PVIm and PVBA–PVIm, and their stepwise uptake of approximately 6  $\text{mmol g}^{-1}$  from Fig. 5a, corresponding to about 1 equivalent of  $\text{NH}_3$  per mol  $-\text{COOH}$  for

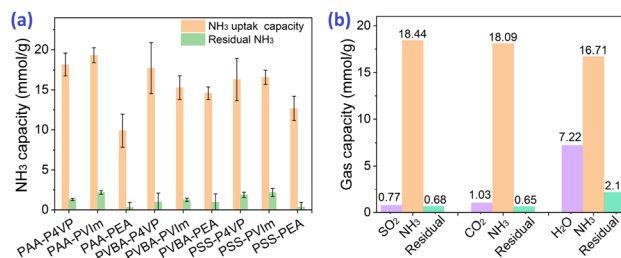


Fig. 4 (a)  $\text{NH}_3$  uptake capacity of the acid–basic hybrid polymers at 25 °C and 1 bar. (b) Staged adsorption of 5%  $\text{SO}_2$  and  $\text{NH}_3$ ,  $\text{CO}_2$  and  $\text{NH}_3$ , as well as 3.1%  $\text{H}_2\text{O}$  and  $\text{NH}_3$  of PAA–P4VP at 25 °C. The residual gases were obtained after desorption in a vacuum at 80 °C for 100 min. The remaining capacity of adsorbate after desorption was converted into  $\text{NH}_3$  gas.





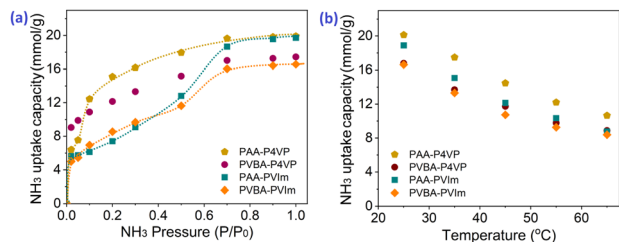


Fig. 5  $\text{NH}_3$  uptake capacity of acid-basic hybrid polymers at various temperatures under 1 bar  $\text{NH}_3$  pressure (a) and under various pressures at 25 °C (b).

the acid-base reaction to  $-\text{COONH}_4$ . Another 10–13  $\text{mmol g}^{-1}$   $\text{NH}_3$  uptake of these hybrid polymers probably contributed to the hydrogen interaction.

### The analysis of $\text{NH}_3$ uptake of acid-base hybrid polymers

The IR spectra of the hybrid polymers compared with their  $\text{NH}_3$  saturated state are shown in Fig. 6. The increase in absorption at about  $3400 \text{ cm}^{-1}$  was due to the N–H stretching of adsorbed ammonia. Another characteristic peak at about  $1470 \text{ cm}^{-1}$  increased after ammonia absorption, which can be attributed to the symmetric deformation of the ammonium ion.<sup>57,58</sup> Meanwhile, the disappearance of  $\nu_s(\text{COOH})$  at about  $1710 \text{ cm}^{-1}$  (marked with \*) and the increase in  $\nu_s(\text{COO}^-)$  and  $\nu_{as}(\text{COO}^-)$  at about  $1520 \text{ cm}^{-1}$  and  $1350 \text{ cm}^{-1}$  (marked with #) indicate the carboxylic acid of hybrid polymers forming the carboxylate salt.<sup>59</sup> These results support the formation of  $\text{NH}_4^+$  from the reaction of  $\text{NH}_3$  with the proton of hybrid polymers.<sup>60</sup> A new peak at about  $910 \text{ cm}^{-1}$  (marked with ▼) is ascribed to the hydrogen bonding of  $\text{NH}_3$  from PAA-PVIm and PVBA-PVIm, while that at  $850 \text{ cm}^{-1}$  was due to PVBA-P4VP.<sup>19</sup> The results claim the hybrid polymers from carboxylic acid polymers and Lewis base polymers achieved high  $\text{NH}_3$  uptake capacity, which is attributed to the cooperative acid-base interaction and hydrogen bonding interactions.

The properties of  $\text{NH}_3$  desorption from the hybrid acid-base polymers were investigated through  $\text{NH}_3$ -TPD measurements. The results presented in Fig. S11† indicate  $\text{NH}_3$  desorption peak

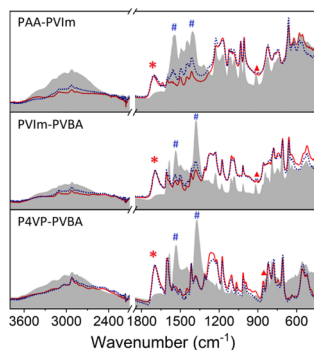


Fig. 6 Comparison of the partial IR spectra of hybrid polymers (red solid line) with their  $\text{NH}_3$  saturated (gray background) and desorbed states (blue dotted lines).

before 100 °C for all these hybrid polymers, the active energy of desorption of  $103.2\text{--}107.6 \text{ kJ mol}^{-1}$  as listed in Table 1, which belonged to the  $\text{NH}_3$  released from the  $\text{NH}_3$  fixed by acid-base interactions. The ammonia trapped by PVBA-P4VP and PVBA-PVIm would be released completely within 200 °C, indicating the feasible desorption of  $\text{NH}_3$  from these hybrid polymers. The IR spectra of the hybrid polymers after the  $\text{NH}_3$ -TPD test compared with the pristine sample in Fig. 6 indicate that carboxylic acid would be recovered after  $\text{NH}_3$  desorption. The reusability of these hybrid polymers for  $\text{NH}_3$  uptake was further investigated. Fig. S12–14† show that the  $\text{NH}_3$  uptake capacity did not decrease within 6 cycles of consecutive  $\text{NH}_3$  uptake and desorption. About  $2.8 \text{ mmol g}^{-1}$   $\text{NH}_3$  remained in PAA-PVIm ( $2.3 \text{ mmol g}^{-1}$   $\text{NH}_3$  remained in PVBA-PVIm) after desorption, which would not affect the subsequent  $\text{NH}_3$  adsorption. The reversibility of these hybrid polymers indicates that the acidic polymer hybrid with appropriate basic polymer is one of the designable strategies to promote  $\text{NH}_3$  desorption and the recovery of hybrid polymers.

## Conclusions

The simple acid-base hybrid polymer PAA-P4VP presents a porous structure and superior  $\text{NH}_3$  uptake properties as compared to PAA for synergetic  $\text{NH}_3$  capture through acid-base and CHB interactions. Inspired by this result, a series of mesoporous acid-base hybrid polymers presenting surface areas of  $11.2$  to  $23.6 \text{ m}^2 \text{ g}^{-1}$  were synthesized according to the predicted interactions between the acidic and basic moieties. These acid-base hybrid polymers were used for efficient  $\text{NH}_3$  uptake with the capacity of  $15.8\text{--}19.3 \text{ mmol NH}_3 \text{ g}^{-1}$  through the cooperative acid-base reaction and hydrogen bonding interactions. The trapped  $\text{NH}_3$  can be released at 80 °C under vacuum along with the reformation of CHBs between the  $-\text{COOH}$  and Lewis base moieties. This indicates that the incorporation of the basic moiety is a feasible method for improving the  $\text{NH}_3$  uptake and desorption of materials with the carboxylic acid groups.

## Author contributions

Conceptualization, Xiaoyan Luo and Congmin Wang; data curation, Yibang Liu; formal analysis, Xiaoyan Luo and Yibang Liu; funding acquisition, Xiaoyan Luo; investigation, Xiaoyan Luo and Yibang Liu; methodology, Yibang Liu and Mingxing Li; project administration, Congmin Wang; resources, Ling Ye, Xuegong Cao and Congmin Wang; software, Xuegong Cao; supervision, Xiaoyan Luo and Congmin Wang; validation, Yibang Liu, Mingxing Li and Renhui Ling; writing – original draft, Xiaoyan Luo; writing – review & editing, Congmin Wang.

## Conflicts of interest

There are no conflicts to declare.

## Acknowledgements

This work was funded by the National Natural Science Foundation of China (21803021, 22278165), Science and Technology



Innovation Funding Project from Huaqiao University (ZQN-PY605). We acknowledge the instrumental analysis center of Huaqiao University.

## References

- 1 D. Barpaga and M. D. LeVan, *Microporous Mesoporous Mater.*, 2016, **221**, 197–203.
- 2 M. R. Adam, M. H. D. Othman, S. H. S. A. Kadir, M. N. M. Sokri, Z. S. Tai, Y. Iwamoto, M. Tanemura, S. Honda, M. H. Puteh, M. A. Rahman and J. Jaafar, *Membranes*, 2020, **10**, 63.
- 3 P. Assawasaengrat and R. Rueangdechawiwat, *IOP Conf. Ser.: Mater. Sci. Eng.*, 2019, **639**, 012050.
- 4 I. Matito-Martos, A. Martin-Calvo, C. O. Ania, J. B. Parra, J. M. Vicent-Luna and S. Calero, *Chem. Eng. J.*, 2020, **387**, 124062.
- 5 A. Gladysiak, Tu N. Nguyen, J. A. R. Navarro, M. J. Rosseinsky and K. C. Stylianou, *Chem. – Eur. J.*, 2017, **23**, 13602–13606.
- 6 A. J. Rieth and M. Dinca, *J. Am. Chem. Soc.*, 2018, **140**, 3461–3466.
- 7 D. W. Kang, M. Kang, M. Moon, H. Kim, S. Eom, J. H. Choe, W. R. Lee and C. S. Hong, *Chem. Sci.*, 2018, **9**, 6871–6877.
- 8 C. J. Doonan, D. J. Tranchemontagne, T. G. Glover, J. R. Hunt and O. M. Yaghi, *Nat. Chem.*, 2010, **2**, 235–238.
- 9 D. W. Kang, M. Kang, H. Kim, J. H. Choe, D. W. Kim, J. R. Park, W. R. Lee, D. Moon and C. S. Hong, *Angew. Chem., Int. Ed.*, 2019, **58**, 16152–16155.
- 10 D. W. Kang, S. E. Ju, D. W. Kim, M. Kang, H. Kim and C. S. Hong, *Adv. Sci.*, 2020, **7**, 2002142.
- 11 W. Morris, C. J. Doonan and O. M. Yaghi, *Inorg. Chem.*, 2011, **50**, 6853–6855.
- 12 J. B. DeCoste, T. J. Demasky, M. J. Katz, O. K. Farha and J. T. Hupp, *New J. Chem.*, 2015, **39**, 2396–2399.
- 13 H. Jasuja, G. W. Peterson, J. B. Decoste, M. A. Browe and K. S. Walton, *Chem. Eng. Sci.*, 2015, **124**, 118–124.
- 14 T. Yoskamtorn, P. Zhao, X. P. Wu, K. Purchase, F. Orlandi, P. Manuel, J. Taylor, Y. Y. Li, S. Day, L. Ye, C. C. Tang, Y. F. Zhao and S. C. E. Tsang, *J. Am. Chem. Soc.*, 2021, **143**, 3205–3218.
- 15 G. Barin, G. W. Peterson, V. Crocella, J. Xu, K. A. Colwell, A. Nandy, J. A. Reimer, S. Bordiga and J. R. Long, *Chem. Sci.*, 2017, **8**, 4399–4409.
- 16 O. T. Wilcox, A. Fateeva, A. P. Katsoulidis, M. W. Smith, C. A. Stone and M. J. Rosseinsky, *Chem. Commun.*, 2015, **51**, 14989–14991.
- 17 S. Moribe, Z. J. Chen, S. Alayoglu, Z. H. Syed, T. Islamoglu and O. K. Farha, *ACS Mater. Lett.*, 2019, **1**, 476–480.
- 18 Y. W. Chen, X. Zhang, K. K. Ma, Z. J. Chen, X. J. Wang, J. Knapp, S. Alayoglu, F. F. Wang, Q. B. Xia, Z. Li, T. Islamoglu and O. K. Farha, *ACS Appl. Nano Mater.*, 2019, **2**, 6098–6102.
- 19 J. Zhang, M. Yongde, W. Wu, Z. Cai, Y. Cao, K. Huang and L. Jiang, *Chem. Eng. J.*, 2022, **448**, 137640.
- 20 J. F. Van Humbeck, T. M. McDonald, X. Jing, B. M. Wiers, G. Zhu and J. R. Long, *J. Am. Chem. Soc.*, 2014, **136**, 2432–2440.
- 21 S. Glomb, D. Woschko, G. Makhoulfi and C. Janiak, *ACS Appl. Mater. Interfaces*, 2017, **9**, 37419–37434.
- 22 I. R.-L. Ricardo Dominguez-Gonzalez, E. Martinez-Ahumada, D. Martinez-Otero, H. A. Lara-Garcia, J. Balmaseda-Era, I. A. Ibarra, E. G. Percastegui and V. Jancik, *J. Mater. Chem. A*, 2019, **6**, 26812.
- 23 J. Palomar, M. Gonzalez-Miquel, J. Bedia, F. Rodriguez and J. J. Rodriguez, *Sep. Purif. Technol.*, 2011, **82**, 43–52.
- 24 D. S. Deng, X. X. Deng, K. Li and H. Fang, *Sep. Purif. Technol.*, 2021, **276**, 119298.
- 25 D. W. Shang, X. P. Zhang, S. J. Zeng, K. Jiang, H. S. Gao, H. F. Dong, Q. Y. Yang and S. J. Zhang, *Green Chem.*, 2017, **19**, 937–945.
- 26 L. Yuan, X. P. Zhang, B. Z. Ren, Y. L. Yang, Y. G. Bai, L. Bai, H. S. Gao and S. J. Zeng, *J. Chem. Technol. Biotechnol.*, 2020, **95**, 1815–1824.
- 27 L. Xia, Q. Cui, X. Suo, Y. Li, X. Cui, Q. Yang, J. Xu, Y. Yang and H. Xing, *Adv. Funct. Mater.*, 2018, **28**, 1704292.
- 28 X. Suo, X. Cui, L. Yang, N. Xu, Y. Huang, Y. He, S. Dai and H. Xing, *Adv. Mater.*, 2020, **32**, 1907601.
- 29 X. Y. Luo, R. X. Qiu, X. Y. Chen, B. Y. Pei, J. Q. Lin and C. M. Wang, *ACS Sustainable Chem. Eng.*, 2019, **7**, 9888–9895.
- 30 R. X. Qiu, X. Y. Luo, L. Yang, J. R. Li, X. Y. Chen, C. Peng and J. Q. Lin, *ACS Sustainable Chem. Eng.*, 2020, **8**, 1637–1643.
- 31 Y. Marcus, *The Variety of Deep Eutectic Solvents*, in *Deep eutectic solvents*, Springer, Cham, 2019, pp. 13–44, DOI: [10.1007/978-3-030-00608-2\\_2](https://doi.org/10.1007/978-3-030-00608-2_2).
- 32 D. Yu and T. Mu, *J. Phys. Chem. B*, 2019, **123**, 4958–4966.
- 33 Q. Zhang, K. De Oliveira Vigier, S. Royer and F. Jerome, *Chem. Soc. Rev.*, 2012, **41**, 7108–7146.
- 34 A. I. Akhmetshina, A. N. Petukhov, A. Mechergui, A. V. Vorotyntsev, A. V. Nyuchev, A. A. Moskvichev and I. V. Vorotyntsev, *J. Chem. Eng. Data*, 2018, **63**, 1896–1904.
- 35 F. Zhong, H. Peng, D. Tao, P. Wu, J. Fan and K. Huang, *ACS Sustain. Chem. Eng.*, 2019, **7**, 3258–3266.
- 36 D. Deng, B. Gao, C. Zhang, X. Duan, Y. Cui and J. Ning, *Chem. Eng. J.*, 2019, **358**, 936–943.
- 37 Z.-L. Li, F.-Y. Zhong, L.-S. Zhou, Z.-Q. Tian and K. Huang, *Ind. Eng. Chem. Res.*, 2020, **59**, 2060–2067.
- 38 D. S. Deng, X. X. Deng, X. Z. Duan and L. Gong, *J. Mol. Liq.*, 2021, **324**, 114719.
- 39 W. Sun, T. Li, H. Chu, J. Liu, K. Zhong and L. Feng, *J. Cleaner Prod.*, 2022, **373**, 133764.
- 40 Y. H. Li, M. C. Ali, Q. W. Yang, Z. G. Zhang, Z. B. Bao, B. G. Su, H. B. Xing and Q. L. Ren, *ChemSusChem*, 2017, **10**, 3368–3377.
- 41 X. Z. Duan, B. Gao, C. Zhang and D. S. Deng, *J. Chem. Thermodyn.*, 2019, **133**, 79–84.
- 42 F. Y. Zhong, K. Huang and H. L. Peng, *J. Chem. Thermodyn.*, 2019, **129**, 5–11.
- 43 F. Y. Zhong, H. L. Peng, D. J. Tao, P. K. Wu, J. P. Fan and K. Huang, *ACS Sustainable Chem. Eng.*, 2019, **7**, 3258–3266.
- 44 N. N. Cheng, Z. L. Li, H. C. Lan, W. L. Xu, W. J. Jiang, K. Huang and H. L. Peng, *Sep. Purif. Technol.*, 2021, **269**, 118791.
- 45 Z. L. Li, F. Y. Zhong, J. Y. Huang, H. L. Peng and K. Huang, *J. Mol. Liq.*, 2020, **317**, 113992.



- 46 D. S. Deng, B. Gao, C. Zhang, X. Z. Duan, Y. H. Cui and J. H. Ning, *Chem. Eng. J.*, 2019, **358**, 936–943.
- 47 K. Li, H. Fang, X. Z. Duan and D. S. Deng, *J. Mol. Liq.*, 2021, **339**, 116724.
- 48 D. S. Deng, X. Z. Duan, B. Gao, C. Zhang, X. X. Deng and L. Gong, *New J. Chem.*, 2019, **43**, 11636–11642.
- 49 F. Y. Zhong, L. S. Zhou, J. Shen, Y. Liu, J. P. Fan and K. Huang, *ACS Sustainable Chem. Eng.*, 2019, **7**, 14170–14171.
- 50 W. J. Jiang, J. B. Zhang, Y. T. Zou, H. L. Peng and K. Huang, *ACS Sustainable Chem. Eng.*, 2020, **8**, 13408–13417.
- 51 Z. L. Li, F. Y. Zhong, L. S. Zhou, Z. Q. Tian and K. Huang, *Ind. Eng. Chem. Res.*, 2020, **59**, 2060–2067.
- 52 K. Li, K. Zong, Z. Y. Zhou and D. S. Deng, *Sep. Purif. Technol.*, 2021, **279**, 119763.
- 53 N. N. Cheng, Z. L. Li, H. C. Lan, W. L. Xu and K. Huang, *AIChE J.*, 2022, **68**, e17660.
- 54 X. X. Sun, Q. H. Wang, S. H. Wu, X. Y. Zhao, L. G. Wei, K. L. Li, J. A. Hao, L. Wei, S. R. Zhai and Q. D. An, *Int. J. Hydrogen Energy*, 2022, **47**, 16121–16131.
- 55 P. A. Redhead, *Vacuum*, 1962, **12**, 203–211.
- 56 B. E. R. Snyder, A. B. Turkiewicz, H. Furukawa, M. V. Paley, E. O. Velasquez, M. N. Dods and J. R. Long, *Nature*, 2023, **613**, 287–291.
- 57 D. W. Kim, D. W. Kang, M. Kang, D. S. Choi, H. Yun, S. Y. Kim, S. M. Lee, J.-H. Lee and C. S. Hong, *J. Am. Chem. Soc.*, 2022, **144**, 9672–9683.
- 58 C. Petit, B. Mendoza and T. J. Bandosz, *Langmuir*, 2010, **26**, 15302–15309.
- 59 X. Kan, Z. Liu, F. Liu, F. Li, W. Chen, X. Yi, A. Zheng, L. Jiang and F.-S. Xiao, *Chem. Eng. J.*, 2023, **451**, 139085.
- 60 D. Jung, Z. Chen, S. Alayoglu, M. R. Mian, T. A. Goetjen, K. B. Idrees, K. O. Kirlikovali, T. Islamoglu and O. K. Farha, *ACS Appl. Mater. Interfaces*, 2021, **13**, 10409–10415.

